

Banner appropriate to article type will appear here in typeset article

Scale invariance of intermittency in LES turbulence

B. Magacho^{1†}, S. Thalabard², M. Buzzicotti³, F. Bonaccorso³, L. Biferale³, A. A. Mailybaev¹

¹Instituto de Matemática Pura e Aplicada – IMPA, Rio de Janeiro, Brazil

²Université Côte d'Azur, CNRS, Institut de Physique de Nice, 06200 Nice, France

³University of Rome "Tor Vergata", Department of Physics and INFN, Rome, Italy

(Received xx; revised xx; accepted xx)

Turbulent flows exhibit large intermittent fluctuations from inertial to dissipative scales, characterized by multifractal statistics and breaking the statistical self-similarity. It has recently been proposed that the Navier-Stokes turbulence restores a hidden form of scale invariance in the inertial interval when formulated for a dynamically (nonlinearly) rescaled quasi-Lagrangian velocity field. Here we show that such hidden self-similarity extends to the Large-Eddy Simulation (LES) approach in computational fluid dynamics (CFD). In particular, we show that classical subgrid-scale models, such as implicit or explicit Smagorinsky closures, respect the hidden scale invariance at all scales – both resolved and subgrid. In the inertial range, they reproduce the hidden scale invariance of Navier-Stokes statistics. These properties are verified very accurately by numerical simulations and, beyond CFD, turn LES into a valuable tool for fundamental turbulence research.

Key words: turbulence, intermittency, large-eddy simulation, hidden symmetry

1. Introduction

Large-eddy simulations are used in applied studies to simulate large-scale turbulent dynamics, relying on empirical modeling at small (subgrid) scales (Pope 2000; Meneveau & Katz 2000; Sagaut 2005; Fureby 2008). They are capable of generating intermittent (multifractal) velocity fields $\mathbf{u}(\mathbf{x}, t)$, reproducing key features of homogeneous 3D turbulence (Cerutti & Meneveau 1998; Biferale *et al.* 2019; Linkmann *et al.* 2018). Classical description of intermittency involves, in particular, the distributions of longitudinal velocity increments $\Delta_\ell u_\parallel = [\mathbf{u}(\mathbf{x} + \ell \mathbf{e}) - \mathbf{u}(\mathbf{x})] \cdot \mathbf{e}$ becoming increasingly flat-tailed at small scales and leading to anomalous scaling of structure functions (Frisch 1995; Chevillard 2015; Iyer *et al.* 2017); see Fig. 1. The multifractal phenomenology is rooted in the scaling symmetries of the Navier-Stokes (NS) equations, suggesting that these symmetries should drive any modeling strategies of turbulence including LES. Here we investigate the Hidden Scale Invariance (HS) approach developed recently by Mailybaev (2022a); Mailybaev & Thalabard (2022), which describes scaling properties of the NS in a quasi-Lagrangian reference frame (Belinicher & L'vov 1987;

† Email address for correspondence: bruno.magacho@impa.br

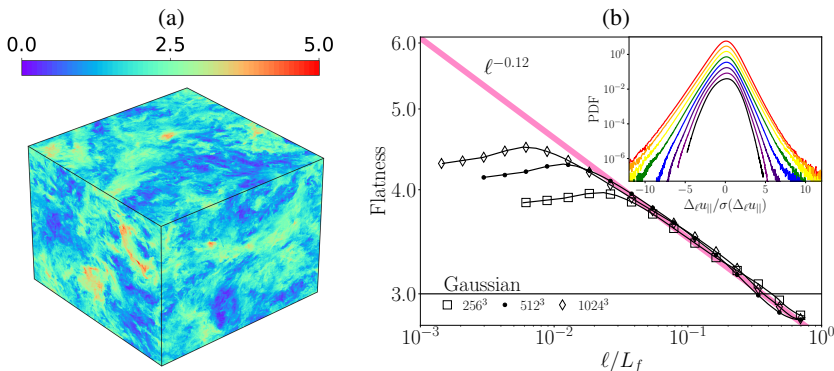


Figure 1: (a) 3D rendering of the velocity norm $|\mathbf{u}|$ in units of the typical velocity $U_f \approx 2.4$ for LES at resolution $N^3 = 1024^3$. (b) Broken self-similarity. Shown is the flatness of the longitudinal velocity increments $\Delta_\ell u_{||}$ for different resolutions; see the *implicit* line in Tab. 1 for numerical details. For reference, in purple we show the anomalous scaling $\propto \ell^{-0.12}$. The inset shows the normalized PDFs (shifted vertically for better visibility) for the 1024^3 run at scales ranging geometrically from δ to 128δ from top to bottom.

Mitra & Pandit 2004; Biferale *et al.* 2011) after dynamic (nonlinear) rescaling. By revealing unbroken (hidden) self-similarity of intermittent statistics, this approach provides theoretical support to the anomalous scaling of structure functions (Mailybaev 2022b; Thalabard & Mailybaev 2024; Calascibetta *et al.* 2025) and the universal statistics of multipliers, the ratios like $\Delta_\ell u_{||} / \Delta_{\ell'} u_{||}$, as conjectured by Kolmogorov’s third hypothesis (Kolmogorov 1962; Chen *et al.* 2003). Extension of the HS to SGS closures has been recently studied in shell models (Mailybaev 2023).

In this work, we prove that properly designed SGS models, for which the Smagorinsky is the simplest example, preserve the HS. This implies that the rescaled quasi-Lagrangian statistics does not depend on the observation scale, ℓ , and the filtering (cut-off) scale, δ , separately but only through their ratio $\alpha = \ell/\delta$. Besides, for those resolved scales inside the inertial range and far from the cut-off, $\delta \ll \ell \ll L_f$, the statistics becomes independent of α and coincides with the analogous hidden-symmetric statistics of the NS. Performing high-resolution simulations, we provide very accurate numerical verification of HS. Such accuracy is attained because the HS in SGS models extends to subgrid scales, unlike the NS where it only refers to the inertial range. This stronger form of HS has implications for both practical (development of SGS models) and theoretical studies of turbulence.

2. Kinematic rescaling of a quasi-Lagrangian velocity

Navier-Stokes-Smagorinsky equation. In practice, the closure problem takes as inputs a filtering scale δ and a filter G . It aims to predict the dynamics of the filtered field as the convolution $\mathbf{u}_\delta = G_\delta * \mathbf{u}$ with the kernel $G_\delta(\mathbf{x}) = \delta^{-3} G(\mathbf{x}/\delta)$, providing implicit or explicit parametrizations for the so-called subgrid scale tensor $\mathbf{R}_\delta = (\mathbf{u} \otimes \mathbf{u})_\delta - \mathbf{u}_\delta \otimes \mathbf{u}_\delta$. We start with the simplest example of the Smagorinsky model, in which \mathbf{R}_δ is expressed as the viscous stress with the effective eddy-viscosity ν_s . Dropping δ ’s from the subscripts, the resulting Navier-Stokes-Smagorinsky (NSS) dynamics for the filtered velocity becomes

$$\partial_t \mathbf{u} + \mathbf{u} \cdot \nabla \mathbf{u} = -\nabla p + \nabla \cdot (2\nu_s \mathbf{s}) + \mathbf{f}, \quad \nabla \cdot \mathbf{u} = 0, \quad (2.1)$$

where $p(\mathbf{x}, t)$ is the pressure and $\mathbf{f}(\mathbf{x}, t)$ is a large-scale force with correlation length $L_f \gg \delta$. The eddy viscosity is defined in terms of the filtered rate-of-strain tensor \mathbf{s} as

$$\nu_s = (c_s \delta)^2 \|\mathbf{s}\|, \quad \mathbf{s} = \frac{1}{2} \left(\nabla \mathbf{u} + (\nabla \mathbf{u})^T \right), \quad (2.2)$$

with the Smagorinsky constant $c_s = 0.1$ and the norm $\|\mathbf{s}\|^2 = \sum 2s_{ij}^2$. Considering the filtering scale δ to be much larger than the viscous scale, the kinematic viscosity $\nu \ll \nu_s$ is small and, therefore, omitted in the NSS equations (2.1). The filtering operation leading to Eq. (2.2) is formal only. While the NSS dynamics aims to mimic the Navier-Stokes (NS) equations for the resolved scales $\ell \gg \delta$, the role of eddy viscosity is to replace the energy transfer at the subgrid scales $\ell \lesssim \delta$ by a dissipative scheme (Cruz & Lamballais 2023).

Kinematic rescaling. Similarly to the NS system previously discussed by Mailybaev (2022a); Mailybaev & Thalabard (2022), the starting point of our study is the projection of the velocity field $\mathbf{u}(\mathbf{x}, t)$ into the rescaled velocity field $\mathbf{U}(\mathbf{X}, \tau)$. At a heuristic level, the new field represents a quasi-Lagrangian velocity increment (Belinicher & L'vov 1987) with a dynamically rescaled amplitude and timeframe. The course of proper time τ is determined by the local level of fluctuations, running fast when the latter are high and slowly otherwise. The rescaling is parametrized by an observational scale ℓ and a label $\mathbf{x}_0 \in \mathbb{R}^3$. The label selects a Lagrangian trajectory as

$$\frac{d\mathbf{x}_*}{dt} = \mathbf{u}(\mathbf{x}_*, t), \quad \mathbf{x}_*(0) = \mathbf{x}_0. \quad (2.3)$$

Fluctuations at scale ℓ are measured as amplitudes of quasi-Lagrangian increments as

$$a_\ell(t) = \sqrt{\int_{|\mathbf{X}| \leq 1} |\Delta_\ell \mathbf{u}(\mathbf{x}_*(t), \mathbf{X}, t)|^2 d^3 \mathbf{X}}, \quad \Delta_\ell \mathbf{u}(\mathbf{x}, \mathbf{X}, t) = \mathbf{u}(\mathbf{x} + \ell \mathbf{X}, t) - \mathbf{u}(\mathbf{x}, t). \quad (2.4)$$

The velocity field is then rescaled as

$$\mathbf{U}(\mathbf{X}, \tau) = \frac{\Delta_\ell \mathbf{u}(\mathbf{x}_*(t), \mathbf{X}, t)}{a_\ell(t)}, \quad \tau = \frac{1}{\ell} \int_0^t a_\ell(s) ds, \quad (2.5)$$

where the second formula introduces the change of time $t \mapsto \tau$ expressed in terms of amplitude $a_\ell(t)$. Physically, τ represents a Lagrangian clock measuring time in terms of the local turnover time $\ell/a_\ell(t)$ encountered along the trajectory $\mathbf{x}_*(t)$.

Switching the observation scale. Changing the scale $\ell \mapsto \ell'$ in Eqs. (2.4) and (2.5) reduces to a specific transformation of the respective fields $\mathbf{U}(\mathbf{X}, \tau) \mapsto \mathbf{U}'(\mathbf{X}, \tau')$ expressed as

$$\mathbf{U}'(\mathbf{X}, \tau') = \frac{\mathbf{U}(\mathbf{X}/\lambda, \tau)}{A(\tau)}, \quad \tau' = \lambda \int_0^{\tau'} A(\tau) ds, \quad A(\tau) = \sqrt{\int_{|\mathbf{X}| \leq 1} |\mathbf{U}(\mathbf{X}/\lambda, \tau)|^2 d^3 \mathbf{X}}, \quad (2.6)$$

where $\lambda = \ell/\ell'$ and the second relation introduces the change of time $\tau \mapsto \tau'$. The kinematic relations (2.5) and (2.6) are demonstrated schematically in Fig. 2(a) by straight and wavy arrows, respectively. In this figure, we specified the parameters in the subscripts: \mathbf{u}_δ for the original field depending on the filtering scale δ and $\mathbf{U}_{\delta, \ell, \mathbf{x}_0}$ for the rescaled field depending additionally on the observation scale ℓ and the label \mathbf{x}_0 .

NSS under kinematic rescaling. The governing equations for the rescaled velocity field $\mathbf{U}(\mathbf{X}, \tau)$ are obtained by differentiating the definition (2.5) with respect to τ and using the NSS system (2.1) and (2.2). The lengthy but elementary derivation yields (see §A.1)

$$\partial_\tau \mathbf{U} = \Lambda_{\mathbf{U}} \left[-\mathbf{U} \cdot \nabla \mathbf{U} - \nabla P + 2c_s^2 \alpha^{-2} \nabla \cdot (\|\mathbf{S}\|\mathbf{S}) + \mathbf{F} \right], \quad \nabla \cdot \mathbf{U} = 0. \quad (2.7)$$

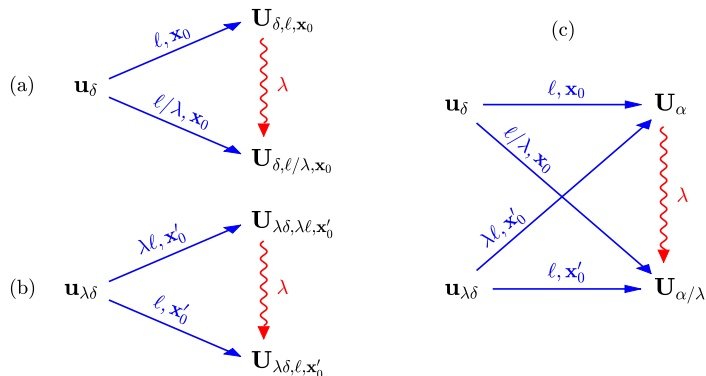


Figure 2: (a) Kinematic rescaling diagram, where the projections (2.5) are shown by straight arrows for two different scales ℓ and $\ell' = \lambda\ell$, and the transformation (2.6) is shown by the wavy arrow. (b) Similar diagram for a different filtering scale $\delta' = \delta/\lambda$. (c) Manifestation of the hidden self-similarity as the fusion of the previous diagrams in their right-hand sides.

Here $\alpha = \ell/\delta$, the tensor $\mathcal{S} = \frac{1}{2}\nabla\mathbf{U} + \frac{1}{2}(\nabla\mathbf{U})^T$, and the gradient operator ∇ acts on the new space variable \mathbf{X} . The operator Λ_U is defined for any field $V(\mathbf{X}, \tau)$ as

$$\Lambda_U[V] = \tilde{V} - U \int_{|\mathbf{X}| \leq 1} U \cdot \tilde{V} d^3\mathbf{X}, \quad \tilde{V} = V(\mathbf{X}, \tau) - V(\mathbf{0}, \tau). \quad (2.8)$$

The rescaled forcing term is expressed, with the times $t \mapsto \tau$ related by Eq. (2.5), as

$$\mathbf{F}(\mathbf{X}, \tau) = \frac{\ell \Delta_\ell \mathbf{f}(\mathbf{x}_*(t), \mathbf{X}, t)}{a_\ell^2(t)}, \quad \Delta_\ell \mathbf{f}(\mathbf{x}, \mathbf{X}, t) = \mathbf{f}(\mathbf{x} + \ell\mathbf{X}, t) - \mathbf{f}(\mathbf{x}, t). \quad (2.9)$$

3. Hidden scale invariance

The limit of small observational scales. System (2.7) governs the dynamics of the new velocity and pressure fields $\mathbf{U}(\mathbf{X}, \tau)$ and $P(\mathbf{X}, \tau)$. It is, however, not closed with respect to these fields, because the coupling with the original dynamics $\mathbf{u}(\mathbf{x}, t)$ permeates through the dependence of forcing term (2.9) on $a_\ell(t)$. We now argue that a closed formulation follows asymptotically at small observational scales $\ell \ll L_f$, in which case the forcing term is negligible. Indeed, we have $\partial_\tau \mathbf{U} \sim 1$ for $\mathbf{X} \sim 1$ by construction from Eqs. (2.4) and (2.5). This implies that the lhs in Eq. (2.7) is ~ 1 . As for the forcing term, we first consider the case $\delta \lesssim \ell \ll L_f$, describing an observational scale in the resolved (turbulent) range. The dimensional estimate $\mathbf{f} \sim U_f^2/L_f$ in Eq. (2.9) yields $\Delta_\ell \mathbf{f} \sim U_f^2 \ell/L_f^2$, with U_f the integral (forcing-scale) velocity. Using the K41 estimate $a_\ell \sim U_f(\ell/L_f)^{1/3}$ for the amplitude of velocity fluctuations in Eq. (2.9), we conclude that the forcing term $\mathbf{F} \sim (\ell/L_f)^{4/3} \ll 1$. This estimate extends to the subgrid range $\ell < \delta \ll L_f$ as $\mathbf{F} \sim (\delta/L_f)^{4/3} \ll 1$.

Therefore, under the condition of small scales $\delta, \ell \ll L_f$, the forcing term can be neglected in the rescaled system (2.7). This gives

$$\delta, \ell \ll L_f : \quad \partial_\tau \mathbf{U} = \Lambda_U \left[-\mathbf{U} \cdot \nabla \mathbf{U} - \nabla P + 2c_s^2 \alpha^{-2} \nabla \cdot (\|\mathcal{S}\| \mathcal{S}) \right], \quad \nabla \cdot \mathbf{U} = 0. \quad (3.10)$$

We call the system (3.10) α -NSS, emphasizing that the dependence on the parameters ℓ and δ is realized only through their ratio $\alpha = \ell/\delta$. Based on these properties, we formulate the hypothesis of *hidden scale invariance*:

For small scales $\ell, \delta \ll L_f$, the statistics of the rescaled field $U(\mathbf{X}, \tau)$, obtained from the NSS solution $\mathbf{u}(\mathbf{x}, t)$, depend on ℓ and δ only through their ratio $\alpha = \ell/\delta$.

Statistical identities. The diagrammatic interpretation of this type of scale invariance is presented in Fig. 2. The panels (a) and (b) show two independent diagrams corresponding to different filtering parameters δ and $\delta' = \lambda\delta$. When viewed at small scales and in a statistical sense, these diagrams merge on their right sides as shown in the panel (c), where U_α denotes a solution of the α -NSS system (3.10). In other terms, the hidden scale invariance is understood as the statistical equivalence

$$U_{\delta, \ell, \mathbf{x}_0} \stackrel{\text{law}}{=} U_{\lambda\delta, \lambda\ell, \mathbf{x}'_0} \stackrel{\text{law}}{=} U_\alpha \quad \text{for } \alpha = \ell/\delta. \quad (3.11)$$

The diagram in Fig. 2(c) also reveals that the rescaled statistics for different values of α and $\alpha' = \alpha/\lambda$ are related by the transformation $h_\lambda : U_\alpha \mapsto U_{\alpha'}$ prescribed by Eq. (2.6). This provides an additional statistical identity

$$U_{\alpha/\lambda} \stackrel{\text{law}}{=} h_\lambda[U_\alpha]. \quad (3.12)$$

HS in the inertial interval. A stronger form of HS develops in the inertial interval, i.e., at scales ℓ defined by the condition $\delta \ll \ell \ll L_f$. Here, the Smagorinsky dissipative term becomes negligible and the system (3.10) simplifies into

$$\delta \ll \ell \ll L : \quad \partial_\tau U + \Lambda_U [U \cdot \nabla U + \nabla P] = 0, \quad \nabla \cdot U = 0. \quad (3.13)$$

This system is independent of both δ and ℓ , and coincides with the rescaled system derived earlier in the framework of NS turbulence by Mailybaev (2022a); Mailybaev & Thalabard (2022). This leads to the hypothesis of *inertial-interval hidden symmetry*:

The statistics of the rescaled field $U(\mathbf{X}, \tau)$ in the inertial interval are universal, i.e. independent of the scale ℓ and the dissipation mechanism.

This suggests that, despite the intermittency, the rescaled NSS and NS statistics coincide at the inertial interval scales. The statistical identity (3.12) in the inertial interval simplifies into

$$U_\infty \stackrel{\text{law}}{=} h_\lambda[U_\infty], \quad (3.14)$$

where U_∞ denotes a solution of system (3.13) obtained in the limit $\alpha \rightarrow \infty$.

HS in other SGS models. We observe that the concept of hidden scale invariance applies equally to hyperviscous Smagorinsky models, such as $\propto \delta^{2p} |\nabla^2|^p \nabla \cdot (\nu_s \mathbf{s})$. More interestingly, modern strategies in LES simulations use implicit dissipation schemes in order to introduce backscattering effects; see, e.g., Pope (2000); Lamballais *et al.* (2021). In practice, these schemes are implemented by under-resolving the NSS through a (genuine) filtering operation, hereby transforming the NSS equations (2.1) into

$$\partial_t \mathbf{u} = (-\mathbf{u} \cdot \nabla \mathbf{u} - \nabla p + \nabla \cdot (2\nu_s \mathbf{s}) + \mathbf{f})_\delta, \quad \nabla \cdot \mathbf{u} = 0, \quad (3.15)$$

where the rhs is the filtered field. Consider the sharp spectral filter $G_\delta(\mathbf{x}) = (2\pi)^{-3} \int_{|\mathbf{k}| \leq c k_\delta} d^3 \mathbf{k} e^{i\mathbf{k} \cdot \mathbf{x}}$ defined as a Galerkin truncation at a given multiple c of the wavenumber $k_\delta = 2\pi/\delta$. Then the kinematic rescaling of §2 yields the filtered α -NSS as

$$\partial_\tau U = (\Lambda_U [-U \cdot \nabla U - \nabla P + 2c_s^2 \alpha^{-2} \nabla \cdot (\|S\|S) + F])_\alpha, \quad \nabla \cdot U = 0 \quad (3.16)$$

(see §A.2). Here the filtering operation $(\dots)_\alpha$ applies wrt the rescaled variable \mathbf{X} at scale $\alpha = \ell/\delta$. Hence, the HS extends to implicit LES schemes. Following Mailybaev (2022a) one can relate the HS of SGS models to their invariance with respect to space-time scaling

	δ	ck_δ	c	Δt
explicit	9.6 Δx	k_{\max}	3.2	0.15/ N
implicit	1.8 Δx	k_{\max}	0.6	0.10/ N

Table 1: Numerical details for two sets of runs with $k_{\max} = N/3$ and $\Delta x = 2\pi/N$ using the filtered NSS Eq. (3.15) at resolutions $N^3 = 256^3, 512^3, 1024^3$. The total integration time is $T_{\max} = 15$ for resolutions up to 512^3 and $T_{\max} = 4.6$ for 1024^3 .

and Galilean symmetry groups. From this point of view, the extension of HS to subgrid (dissipative) scales refers to the time-scale-invariant (quadratic in velocity) SGS model. On the contrary, the HS is limited to the inertial scales of the NS, because physical viscosity breaks the time-scale invariance (Mailybaev & Thalabard 2022).

4. Numerical verification of the hidden scale invariance

Numerical setup. We probe the hidden self-similarity conjectures through direct numerical simulations of the NSS in a triply 2π -periodic domain. Our simulations use a pseudospectral scheme with 2/3-rule dealiasing (Orszag 1971) and a second-order Adam-Bashforth time integration with step Δt . The forcing $\mathbf{f}(\mathbf{x}, t) = \nabla \times \psi$ is specified through the stream vector $\psi = \sqrt{\epsilon} \sum_{1 \leq |\mathbf{k}| \leq 2\pi/L_f} e^{i\mathbf{k} \cdot \mathbf{x}} \boldsymbol{\eta}(\mathbf{k}, t) / (\sum_{1 \leq |\mathbf{k}| \leq 2\pi/L_f} |\mathbf{k}|^2)$. Here $\epsilon = 0.14$ and $L_f = 4\pi/3$ are the energy injection rate and scale, and $\boldsymbol{\eta}(\mathbf{k}, t)$ are white-in-time independent complex standard Gaussian random vectors satisfying the Hermitian symmetry $\boldsymbol{\eta}(\mathbf{k}) = \boldsymbol{\eta}^*(-\mathbf{k})$. We describe two sets of runs with resolution N ranging from 256^3 to 1024^3 , referred to as explicit and implicit runs. In the explicit runs use $\delta \gg \Delta x$ ensuring that dissipation in the subgrid range is dominated by the Smagorinsky damping term, while the implicit runs use $\delta \sim \Delta x$ and allow for energy backscatter; see Table 1 for more details. For numerical convenience we use $|\mathbf{X}| = \max_j |X_j|$ in the amplitudes (2.4) corresponding to averages in a cube.

Temporal averages. The statistics of the rescaled field $\mathbf{U}(\mathbf{X}, \tau)$ can be accessed using different observables. In this work we limit our analysis to the longitudinal component $U_{\parallel}(\tau) = \mathbf{U}(\mathbf{e}, \tau) \cdot \mathbf{e}$ with the unit vector $\mathbf{e} = (1, 0, 0)$; other observables (not presented here) were also tested with similar conclusions. The τ -average of U_{\parallel} is defined as

$$\langle U_{\parallel}(\tau) \rangle_{\tau} = \lim_{T \rightarrow \infty} \frac{1}{T} \int_0^T U_{\parallel}(\tau) d\tau. \quad (4.17)$$

Similarly, we define any moment $\langle |U_{\parallel}(\tau)|^p \rangle_{\tau}$, from which the usual statistical properties such as variance, skewness, flatness, etc. are estimated. The corresponding probability density function (PDF) is obtained from the average of the Dirac delta function as $p_{\parallel}(y) = \langle \delta(U_{\parallel}(\tau) - y) \rangle_{\tau}$. We emphasize that the average (4.17) is expressed in terms of the rescaled Lagrangian clock τ . However, it can be efficiently estimated as space-time average over the original fields using a conversion formula relying on spatial homogeneity and incompressibility. For U_{\parallel} the conversion formula states

$$\langle U_{\parallel}(\tau) \rangle_{\tau} = \left\langle \frac{\Delta_{\ell} u_{\parallel}(\mathbf{x}, t)}{a(\mathbf{x}, t)} J(\mathbf{x}, t) \right\rangle_{\mathbf{x}, t}, \quad (4.18)$$

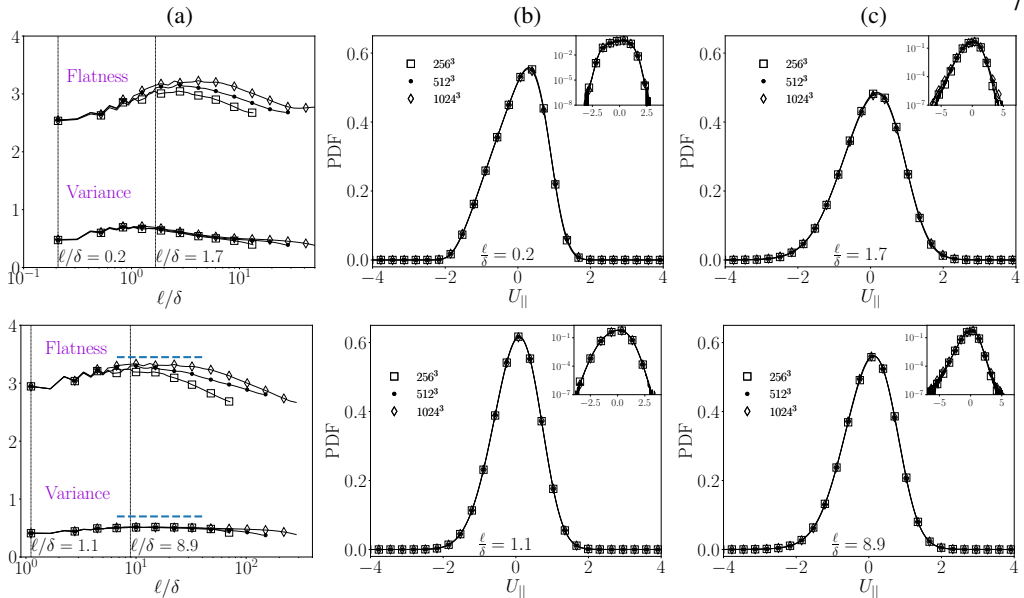


Figure 3: (a) Variance and flatness of the rescaled field component U_{\parallel} as a function of $\alpha = \ell/\delta$. (b,c) PDF of U_{\parallel} at two selected values of ℓ/δ indicated by vertical lines in the left panel. Top and bottom panels use, respectively, the explicit and implicit simulations.

where $\langle \cdot \rangle_{x,t}$ denotes the space-time average in the original coordinates and $\Delta_{\ell} u_{\parallel} = (\mathbf{u}(\mathbf{x} + \ell \mathbf{e}) - \mathbf{u}(\mathbf{x})) \cdot \mathbf{e}$. Here $J(\mathbf{x}, t)$ is the Jacobian factor due to the change of time $\tau \mapsto t$ as

$$J(\mathbf{x}, t) = \frac{a^{-1}(\mathbf{x}, t)}{\langle a^{-1}(\mathbf{x}, t) \rangle_{x,t}}, \quad a^{-1}(\mathbf{x}, t) = \left(\int_{|\mathbf{X}| \leq 1} |\Delta_{\ell} \mathbf{u}(\mathbf{x}, \mathbf{X}, t)|^2 d^3 \mathbf{X} \right)^{-1/2}. \quad (4.19)$$

We refer to [Mailybaev & Thalabard \(2022\)](#) for technical details of this derivation. Expressions similar to Eq. (4.18) follow for other single-time observables.

Numerical results. Figure 3(a) shows the computed variance and flatness of $U_{\parallel}(\tau)$ as functions of $\alpha = \ell/\delta$. Here the top and bottom panels correspond to the explicit and implicit runs, respectively, and we recall that different resolutions feature different δ ; see Tab. 1. In both cases, the curves collapse at small scales (on their left sides), verifying the hidden self-similarity: the statistics depend only on the ratio ℓ/δ . These graphs diverge on their right sides, because the HS gets broken at large (forcing) scales. Panels (b) and (c) illustrate the HS by verifying the collapse at the level of PDFs of U_{\parallel} . We point out the close-to-perfect superposition between different resolutions, representing different ℓ and δ at fixed ratio ℓ/δ .

Explicit runs use large δ and therefore do not develop the inertial range; their HS applies to dissipative scales only. Implicit runs have smaller δ , and a pronounced inertial interval develops at the resolution 1024^3 for the scales $6 \lesssim \ell/\delta \lesssim 42$; see the plateau in the bottom Fig. 3(a). Note that the curves do not collapse well in this range because the inertial interval is shorter for lower resolutions. PDFs of U_{\parallel} for 18 different scales ℓ from the inertial interval are shown by solid lines in Fig. 4(a); these scales correspond to full black squares in Fig. 4(b). These PDFs are visually indistinguishable, confirming the inertial-interval HS. The collapse is quantified in Fig. 4(b), where the black squares show the L_2 -distance between the PDF at scale ℓ and reference PDF from the middle of the inertial interval.

We further test the universality of inertial-interval HS with respect to the dissipation mechanism. For this purpose, we superpose our results with the data obtained from the NS

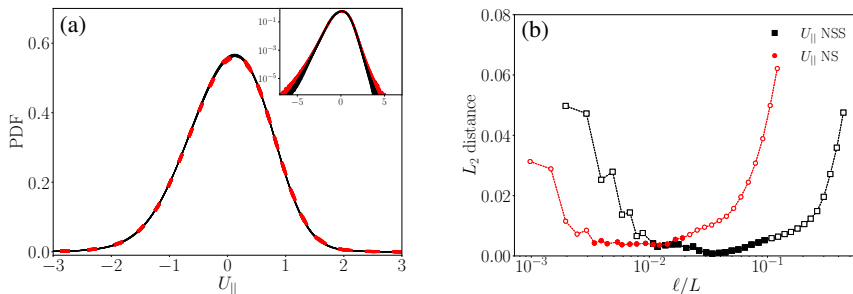


Figure 4: (a) Solid lines represent 18 PDFs of U_{\parallel} for the 1024^3 implicit run; see full black square in the right panel. Red dashed lines present 13 PDFs of U_{\parallel} for the JHU 8192^3 NS simulation; see full red circles in the right panel. (b) L_2 -distance between the PDFs of the left panel and the reference NSS PDF from the middle of the inertial interval.

simulations of the JHU turbulence database at $N = 8192^3$ (Li *et al.* 2008; Yeung *et al.* 2012, 2015). The 13 undistinguishable dashed red lines in Fig.4(a) are the PDFs of U_{\parallel} for different scales from the inertial interval; see the full red dots in the right panel. The close-to-perfect superposition of the PDFs for the NSS and NS simulations confirms the universality of inertial-interval HS. Red circles in Fig. 4(b) quantify this collapse by measuring L_2 -distance between the NS PDF at scale ℓ and the same reference PDF from the NSS data. It is remarkable that the NS inertial interval is shorter despite of much higher resolution.

5. Concluding remarks

Similar to the NS case, the hidden scale invariance of classical LES models involves a quasi-Lagrangian formulation, in which the timeframe is adjusted dynamically to an amplitude of local fluctuations at a scale ℓ . Statistics of the resulting field depend on the observation scale ℓ and on the filtering scale δ only through their ratio ℓ/δ . They become universal in the inertial interval, i.e. independent of both ℓ and δ and coincident with the analogous statistics of 3D Navier-Stokes turbulence. The validity of the hidden scale invariance at both inertial and dissipative scales in the SGS models, in contrast to its restriction to inertial scales only for the NS, allows a very accurate numerical verification of the hidden self-similarity and makes LES useful for the theoretical study of intermittency in turbulence. In particular, LES can be used to test the Perron-Frobenius approach to anomalous scaling previously developed for shell models (Mailybaev 2022b, 2023; Thalabard & Mailybaev 2024) and 2D passive scalar turbulence (Calascibetta *et al.* 2025). The hidden self-similarity across the entire small-scale range may also have applications to the design and optimization of SGS models; see (Biferale *et al.* 2017; Domingues Lemos & Mailybaev 2024; Freitas *et al.* 2025) for similar studies in shell models.

Funding. This work was supported by the European Research Council (ERC) under the European Union’s Horizon 2020 research and innovation program (Grant 882340), CNPq grants 308721/2021-7 and 150944/2024-1, FAPERJ grant E-26/201.054/2022, CAPES grant AMSUD3169225P, and the Brazilian-French Network in Mathematics.

Declaration of interests. The authors report no conflict of interest.

Data availability statement. The data that support the findings of this study are openly available in HS LES Turbulence at <http://doi.org/10.5281/zenodo.15200263>, reference number 15200263. See JFM’s [research transparency policy](#) for more information

A. Appendix

A.1. Derivation of the rescaled system (2.7)

For technical derivations, we drop the subscript ℓ and use the shorthand for Eq. (2.4) as

$$a(t) = \sqrt{\int_{|\mathbf{X}| \leq 1} \mathbf{v} \cdot \mathbf{v} d^3 \mathbf{X}}, \quad \mathbf{v}(\mathbf{X}, t) = \mathbf{u}(\mathbf{x}_*(t) + \ell \mathbf{X}, t) - \mathbf{u}(\mathbf{x}_*(t), t). \quad (\text{A } 1)$$

Differentiating the first equality in Eq. (2.5) with $d\tau = a(t)dt/\ell$ yields

$$\partial_\tau \mathbf{U} = \frac{\ell}{a} \frac{\partial}{\partial t} \frac{\mathbf{v}}{a} = \frac{\ell}{a^2} \frac{\partial \mathbf{v}}{\partial t} - \frac{\ell \mathbf{v}}{a^3} \frac{da}{dt} = \frac{\ell}{a^2} \frac{\partial \mathbf{v}}{\partial t} - \frac{\mathbf{v}}{a} \int_{|\mathbf{X}| \leq 1} \frac{\mathbf{v}}{a} \cdot \left(\frac{\ell}{a^2} \frac{\partial \mathbf{v}}{\partial t} \right) d^3 \mathbf{X}, \quad (\text{A } 2)$$

where we expressed da/dt from Eq. (A 1) and rearranged the factors. Differentiating the second expression in Eq. (A 1) with the chain rule and Eq. (2.3) yields

$$\begin{aligned} \frac{\partial \mathbf{v}}{\partial t} = \mathbf{u} \Big|_{\mathbf{x}_*(t), t} \cdot (\nabla \mathbf{u}) \Big|_{\mathbf{x}_*(t), t}^{\mathbf{x}_*(t) + \ell \mathbf{X}, t} + \frac{\partial \mathbf{u}}{\partial t} \Big|_{\mathbf{x}_*(t), t}^{\mathbf{x}_*(t) + \ell \mathbf{X}, t} &= \mathbf{u} \Big|_{\mathbf{x}_*(t), t} \cdot (\nabla \mathbf{u}) \Big|_{\mathbf{x}_*(t), t}^{\mathbf{x}_*(t) + \ell \mathbf{X}, t} \\ &+ (-\mathbf{u} \cdot \nabla \mathbf{u} - \nabla p + 2(c_s \delta)^2 \nabla \cdot (\|s\|s) + \mathbf{f}) \Big|_{\mathbf{x}_*(t), t}^{\mathbf{x}_*(t) + \ell \mathbf{X}, t}, \end{aligned} \quad (\text{A } 3)$$

where the last equality used the time derivative from Eqs. (2.1) and (2.2). Using Eqs. (A 1) and (2.5) one can check that

$$\mathbf{u} \Big|_{\mathbf{x}_*(t), t} \cdot (\nabla \mathbf{u}) \Big|_{\mathbf{x}_*(t), t}^{\mathbf{x}_*(t) + \ell \mathbf{X}, t} - (\mathbf{u} \cdot \nabla \mathbf{u}) \Big|_{\mathbf{x}_*(t), t}^{\mathbf{x}_*(t) + \ell \mathbf{X}, t} = -\frac{1}{\ell} (\mathbf{v} \cdot \nabla_{\mathbf{X}} \mathbf{v}) \Big|_{\mathbf{0}, t}^{\mathbf{X}, t}, \quad (\text{A } 4)$$

where we distinguished the gradient $\nabla_{\mathbf{X}}$ in the \mathbf{X} space. Similarly,

$$[\nabla \cdot (\|s\|s)] \Big|_{\mathbf{x}_*(t), t}^{\mathbf{x}_*(t) + \ell \mathbf{X}, t} = \frac{1}{\ell^3} [\nabla_{\mathbf{X}} \cdot (\|\tilde{s}\|\tilde{s})] \Big|_{\mathbf{0}, t}^{\mathbf{X}, t}, \quad (\text{A } 5)$$

for the tensors $\mathbf{s} = \frac{1}{2} \nabla \mathbf{u} + \frac{1}{2} (\nabla \mathbf{u})^T$ and $\tilde{\mathbf{s}} = \frac{1}{2} \nabla_{\mathbf{X}} \mathbf{v} + \frac{1}{2} (\nabla_{\mathbf{X}} \mathbf{v})^T$. One can check now that the rescaled system (2.7) with the operator (2.8) follows from Eq. (A 2) after the substitutions of $\mathbf{v}/a = \mathbf{U}$ and the time derivative (A 3) with the terms expressed from Eqs. (A 4), (A 5), the rescaled pressure $P(\mathbf{X}, \tau) = p(\mathbf{x}_*(t) + \ell \mathbf{X}, t)/a^2(t)$ and the forcing term (2.9).

A.2. Derivation of the rescaled system (3.16)

Finally, let us consider a velocity satisfying the NSS (3.15) convolved by the sharp spectral filter $G_\delta(\mathbf{x}) = (2\pi)^{-3} \int_{|\mathbf{k}| \leq c k_\delta} d^3 \mathbf{k} e^{i\mathbf{k} \cdot \mathbf{x}}$ with $k_\delta = 2\pi/\delta$. The steps yielding the rescaled dynamics in Eq. (3.16) are similar, but now one should additionally deal with the filtered terms. One can see that Eqs. (A 1) and (A 2) remain valid, while the last term in Eq. (A 3) gains the filter $(\dots)_\delta \Big|_{\mathbf{x}_*(t), t}^{\mathbf{x}_*(t) + \ell \mathbf{X}, t}$. Next one can check that Eq. (A 4) becomes

$$\mathbf{u} \Big|_{\mathbf{x}_*(t), t} \cdot (\nabla \mathbf{u}) \Big|_{\mathbf{x}_*(t), t}^{\mathbf{x}_*(t) + \ell \mathbf{X}, t} - (\mathbf{u} \cdot \nabla \mathbf{u})_\delta \Big|_{\mathbf{x}_*(t), t}^{\mathbf{x}_*(t) + \ell \mathbf{X}, t} = -\frac{1}{\ell} (\mathbf{v} \cdot \nabla_{\mathbf{X}} \mathbf{v}) \Big|_{\mathbf{0}, t}^{\mathbf{X}, t}. \quad (\text{A } 6)$$

Derivation of this relation is the most technical part: it uses the properties $G_\delta * \mathbf{u} = \mathbf{u}$ and $G_\delta * \nabla \mathbf{u} = \nabla \mathbf{u}$ with proper changes of variables $\mathbf{x} \mapsto \mathbf{X}$ in filter integrals. Verifying also the filtered version of Eq. (A 5), one completes the derivation in a similar way. We leave the remaining details as an exercise.

REFERENCES

- BELINICHER, V. I. & L'VOV, V. S. 1987 A scale-invariant theory of fully developed hydrodynamic turbulence. *Sov. Phys. JETP* **66** (2), 303–313.

- BIFERALE, L., BONACCORSO, F., BUZZICOTTI, M. & IYER, K. 2019 Self-similar subgrid-scale models for inertial range turbulence and accurate measurements of intermittency. *Phys.Rev.Lett.* **123** (1), 014503.
- BIFERALE, L., CALZAVARINI, E. & TOSCHI, F. 2011 Multi-time multi-scale correlation functions in hydrodynamic turbulence. *Physics of Fluids* **23** (8).
- BIFERALE, L., MAILYBAEV, A.A. & PARISI, G. 2017 Optimal subgrid scheme for shell models of turbulence. *Phys. Rev. E* **95**, 043108.
- CALASCIBETTA, C., BIFERALE, L., BONACCORSO, F., CENCINI, M. & MAILYBAEV, A. A. 2025 Hidden symmetry in passive scalar advected by 2D Navier-Stokes turbulence. *Preprint ArXiv:2504.11616* .
- CERUTTI, S. & MENEVEAU, C. 1998 Intermittency and relative scaling of subgrid-scale energy dissipation in isotropic turbulence. *Phys. Fluids* **10** (4), 928–937.
- CHEN, Q., CHEN, S., EYINK, G. & SREENIVASAN, K. 2003 Kolmogorov’s third hypothesis and turbulent sign statistics. *Phys. Rev. Lett.* **90** (25), 254501.
- CHEVILLARD, L. 2015 Une peinture aléatoire de la turbulence des fluides. HDR thesis, ENS Lyon.
- CRUZ, V. & LAMBALLAIS, E. 2023 Physical/numerical duality of explicit/implicit subgrid-scale modelling. *J. Turb.* **24** (6-7), 235–279.
- DOMINGUES LEMOS, J. & MAILYBAEV, A. A. 2024 Data-based approach for time-correlated closures of turbulence models. *Physical Review E* **109** (2), 025101.
- FREITAS, A., UM, K., DESBRUN, M., BUZZICOTTI, M. & BIFERALE, L. 2025 A posteriori closure of turbulence models: are symmetries preserved? *Preprint arXiv:2504.03870* .
- FRISCH, U. 1995 *Turbulence: the legacy of AN Kolmogorov*. Cambridge Univ. Press.
- FUREBY, C. 2008 Towards the use of large eddy simulation in engineering. *Prog. Aerosp. Sci.* **44** (6), 381–396.
- IYER, K., SREENIVASAN, K. & YEUNG, P.-K. 2017 Reynolds number scaling of velocity increments in isotropic turbulence. *Phys. Rev. E* **95** (2), 021101.
- KOLMOGOROV, A. N. 1962 A refinement of previous hypotheses concerning the local structure of turbulence in a viscous incompressible fluid at high reynolds number. *J. Fluid Mech.* **13** (1), 82–85.
- LAMBALLAIS, E., CRUZ, R. & PERRIN, R. 2021 Viscous and hyperviscous filtering for direct and large-eddy simulation. *J. Comp. Phys.* **431**, 110115.
- LI, Y., PERLMAN, E., WAN, M., YANG, Y., MENEVEAU, C., BURNS, R., CHEN, S., SZALAY, A. & EYINK, G. 2008 A public turbulence database cluster and applications to study lagrangian evolution of velocity increments in turbulence. *J. Turb.* (9), N31.
- LINKMANN, M., BUZZICOTTI, M. & BIFERALE, L. 2018 Multi-scale properties of large eddy simulations: correlations between resolved-scale velocity-field increments and subgrid-scale quantities. *Journal of Turbulence* **19** (6), 493–527.
- MAILYBAEV, A. A. 2022a Hidden spatiotemporal symmetries and intermittency in turbulence. *Nonlinearity* **35** (7), 3630–3679.
- MAILYBAEV, A. A. 2022b Shell model intermittency is the hidden self-similarity. *Phys.Rev.Fluids* **7**, 034604.
- MAILYBAEV, A. A. 2023 Hidden scale invariance of turbulence in a shell model: From forcing to dissipation scales. *Physical Review Fluids* **8** (5), 054605.
- MAILYBAEV, A. A. & THALABARD, S. 2022 Hidden scale invariance in Navier–Stokes intermittency. *Philosophical Transactions of the Royal Society A* **380** (2218).
- MENEVEAU, C. & KATZ, J. 2000 Scale-invariance and turbulence models for large-eddy simulation. *Ann. Rev. Fluid Mech.* **32** (1), 1–32.
- MITRA, D. & PANDIT, R. 2004 Varieties of dynamic multiscaling in fluid turbulence. *Phys.Rev.Lett.* **93**, 024501.
- ORSZAG, S. 1971 On the elimination of aliasing in finite-difference schemes by filtering high-wavenumber components. *J. Atmos. Sci.* **28** (6), 1074–1074.
- POPE, S. B. 2000 *Turbulent Flows*. Cambridge Univ. Press.
- SAGAUT, P. 2005 *Large eddy simulation for incompressible flows: an introduction*. Springer.
- THALABARD, S. & MAILYBAEV, A. 2024 From zero-mode intermittency to hidden symmetry in random scalar advection. *J. Stat. Phys.* **191** (131).
- YEUNG, P.-K., DONZIS, D. & SREENIVASAN, K. 2012 Dissipation, enstrophy and pressure statistics in turbulence simulations at high reynolds numbers. *J. Fluid Mech.* **700**, 5–15.
- YEUNG, P.-K., ZHAI, X. & SREENIVASAN, K. 2015 Extreme events in computational turbulence. *Proc. Nat. Ac. Sci.* **112** (41), 12633–12638.